

A novel three-dimensional chaotic system with double wings and spiral chaos: Applications in ship radiation noise detection

Hong Yang(杨宏), Shijia Wang(王世佳), Guohui Li(李国辉)

Citation: Chin. Phys. B. 35, 090506 (2026). DOI: 10.1088/1674-1056/ae111c | CSTR: 32038.14.CPB.ae111c
http://cpb.iphy.ac.cn; http://iopscience.iop.org/cpb

What follows is a list of articles you may be interested in

Multistability and offset boosting in a fractional-order discrete memristive neuron model with application to image encryption

Haneche Nabil, Hamaizia Tayeb

Chin. Phys. B. 35, 080504 (2026). DOI: 10.1088/1674-1056/ae1454 | CSTR: 32038.14.CPB.ae1454

Firing dynamics in a second-order memcapacitor-based FitzHugh–Nagumo neuron with multiscale memory

Zhijun Li(李志军), Pengyang Li(李鹏洋)

Chin. Phys. B. 35, 060505 (2026). DOI: 10.1088/1674-1056/ae4c6b | CSTR: 32038.14.CPB.ae4c6b

Meminductor synaptic coupling in a heterogeneous HR–FHN neuron network: Model, dynamics, and DSP implementation

Yang Yin(尹扬), Zhijun Li(李志军)

Chin. Phys. B. 35, 060503 (2026). DOI: 10.1088/1674-1056/ae56e2 | CSTR: 32038.14.CPB.ae56e2

Fixed points as regulatory hubs in discrete memristive neural networks: An analysis of the FitzHugh–Nagumo model

Shaobo He(贺少波), Jiawei Xiao(肖佳伟), Qilai Chen(陈祺来), Huihai Wang(王会海)

Chin. Phys. B. 35, 060502 (2026). DOI: 10.1088/1674-1056/ae3131 | CSTR: 32038.14.CPB.ae3131

Chaotic bursting and burst synchronization in a discrete dual-Rulkov neural network with memristive synaptic coupling

Ke Meng(孟珂), Yifan Bu(卜一帆), Yinghong Cao(曹颖鸿), Suo Gao(高锁), Qi Li(李琦), Chunpeng Wang(王春鹏), Jun Mou(牟俊)

Chin. Phys. B. 35, 060501 (2026). DOI: 10.1088/1674-1056/ae5f06 | CSTR: 32038.14.CPB.ae5f06

A novel three-dimensional chaotic system with double wings and spiral chaos: Applications in ship radiation noise detection

Hong Yang(杨宏)[†], Shijia Wang(王世佳), and Guohui Li(李国辉)

School of Electronic Engineering, Xi′an University of Posts and Telecommunications, Xi′an 710121, *China*

(Received 21 August 2025; revised manuscript received 4 October 2025; accepted manuscript online 9 October 2025)

Aiming at the deficiency of a traditional two-dimensional chaotic system in detection performance, a three-dimensional double-wing chaotic system (3DDWCS) with a sine term is proposed and applied to the detection of ship radiated noise (SRN). Firstly, the nonlinear characteristics of 3DDWCS are analyzed in detail, such as bifurcation, Lyapunov exponent and equilibrium point. Secondly, fractional-order calculus is introduced into 3DDWCS, and a fractional-order 3D double-wing chaotic system (FO3DDWCS) is proposed. The critical threshold of FO3DDWCS is determined by the bifurcation diagram and verified by phase trajectory. Thirdly, in the performance analysis experiment, the signal-to-noise ratio (SNR) threshold of FO3DDWCS considering the fractional-order derivative is −124.94 dB, which is obviously superior to the integer-order 3D chaotic system and the improved fractional-order chaotic system based on a Duffing oscillator in noise immunity. It has a good detection effect and realizes the detection of signals under the ultra-low SNR threshold. Finally, a weak signal detection method based on FO3DDWCS is proposed and successfully applied to the detection of multi-line spectral periodic signals, distorted signals, SRN and marine biological signal, which verifies the effectiveness and practicability of the proposed detection method.

Keywords: chaotic system, fractional-order, detection, weak signal, ship radiated noise, critical threshold

PACS: 05.45.–a, 05.45.Jn, 05.40.Ca

DOI: 10.1088/1674-1056/ae111c **CSTR:** 32038.14.CPB.ae111c

1. Introduction

The detection of ship radiated noise (SRN) is an important topic in the field of marine acoustics. In-depth research on this topic will not only help improve military monitoring and security protection capabilities, but also help improve environmental protection, technological innovation, international cooperation, and many other aspects.[1] However, the sound level of SRN is getting weaker with the continuous progress of ship stealth technology,[2] resulting in the signal-to-noise ratio (SNR) threshold of the existing detection system being unable to meet the detection requirements. Therefore, it is necessary to study an effective method that can detect the frequency of SRN under ultra-low SNR threshold.

Nowadays, signal detection based on chaos theory has matured and is widely used in many fields such as biomedical signal analysis,[3] communication technology research,[4] bearing fault diagnosis,[5] and underwater target detection.[6,7] Chaos theory uses the characteristics of a chaotic system, which is sensitive to initial value and resistant to noise, to detect signals. It can achieve high-sensitivity detection while suppressing noise. Traditional chaotic systems commonly used to detect weak signals include the Duffing chaotic system[8] and the Van der Pol chaotic system,[9] but it is difficult for these chaotic systems to meet the detection requirements. Therefore, scholars have lowered the SNR threshold of the detection system by coupling or differentiating traditional chaotic systems and introducing fractional-order derivatives or high-order terms into traditional chaotic systems, such as the strongly coupled Duffing–Van der Pol oscillator,[10] the fractional-order double-coupled oscillator (FODCDS),[11] and the new coupled Duffing–Van der Pol system.[12] The detection SNR thresholds of these improved systems have been reduced, but it is still difficult to detect weak signals under the ultra-low SNR threshold.

In recent years, many three-dimensional (3D) non-autonomous chaotic systems have been proposed and applied to weak signal detection research. For example, Yang *et al.* proposed a double vortex chaotic system and used it to detect SRN, which provided a new technical means for underwater target detection.[13] Shen *et al.* proposed two 3D nonautonomous chaotic systems and applied them to underwater weak target detection, completing the goal of detecting signal frequency under ultra-low SNR thresholds.[14,15] Liu *et al.* proposed an improved Liu chaotic system and used it to detect weak signals, solving the problem of output signal waveform not converging.[16] Yan *et al.* proposed a new type of two-wing chaotic system with infinite balance and coexisting rotating attractors, which uses the periodicity of the change in the number of wings to detect weak signals, providing a new detection idea.[17] These detection methods based on 3D non-autonomous chaotic systems have shown good detection results and provided new detection ideas for various traditional detection methods based on improved Duffing oscilla-

[†]Corresponding author. E-mail: uestcyhong@163.com

© 2026 Chinese Physical Society and IOP Publishing Ltd. All rights, including for text and data mining, AI training, and similar technologies, are reserved.

tors. Furthermore, the dynamic behavior of multi-wings and multi-vortexes in chaotic systems is also a key area of research for scholars.[18–21]

Conventional calculus pays attention to integer-order derivatives and integrals, while fractional-order calculus expands this concept by defining the order of derivatives and integrals as fractions. Fractional-order calculus is more accurate in describing physical phenomena, more practical in modeling complex systems, and can provide new solutions to problems that are difficult to solve with integer-order calculus.[22] At present, fractional-order calculus has become a research hotspot. Its application fields are expanding and deepening.[23,24] Therefore, many scholars have applied fractional-order calculus theory to chaotic systems and conducted studies on fractional-order chaotic systems. For example, the fractional-order Lorenz system,[25] fractional-order Rössler system[26] and fractional-order Jerk system,[27] etc. At the same time, some scholars have combined fractional-order calculus with a traditional chaotic system to detect weak signals, such as an incommensurate fractional-order Duffing system,[28] a fractional-order Duffing–Van der Pol oscillator (FODVP),[29] a fractional-order high-order Duffing coupled Van der Pol oscillator (FOHOD-VPO),[30] etc. Compared with the original integer-order chaotic systems, these fractional-order chaotic systems have richer dynamic behaviors, lower detection SNR thresholds and better anti-noise performance, and have good detection effects. However, the introduction of fractional-order calculus into a 3D chaotic system and its application in the detection of weak signals has just begun and needs further research.

In summary, some problems still exist within the current methods of detecting weak signals based on chaotic systems: (i) Traditional chaotic systems still cannot meet the detection requirements in practical applications. (ii) The introduction of fractional-order calculus into 3D chaotic systems and its application in weak signal detection has just started, which needs further in-depth study. In order to detect weak signals under an ultra-low SNR threshold, the fractional-order 3D double-wing chaotic system (FO3DDWCS) is proposed and applied to the detection of SRN. Major contributions of this paper are summarized as follows.

(1) Aiming at the problem that traditional chaotic systems are difficult to meet detection requirements, the 3D double-wing chaotic system (3DDWCS) with a sine term is proposed. The nonlinear characteristics of 3DDWCS are analyzed in detail, and a Simulink simulation model of 3DDWCS is established and run.

(2) Aiming at the problem that the anti-noise performance of 3DDWCS is not ideal, fractional-order calculus is introduced, and FO3DDWCS is proposed. The performance of the system is studied, and the influence of the fractional order on the system is analyzed.

(3) Aiming at the problem that weak signals are difficult to detect under an ultra-low SNR threshold, a weak signal detection method based on FO3DDWCS is proposed and applied to the detection of multi-line spectrum periodic signals, distorted signals, and SRN.

This paper is organized as follows: Section 2 analyzes the proposed 3DDWCS. Section 3 introduces fractional-order calculus, proposes FO3DDWCS, analyzes the choice of fractional order, and determines the critical threshold of the system. In Section 4, a detection method based on FO3DDWCS is proposed, and the detection experiments of analog signals and SRN are carried out. Section 5 discusses the limitations of the proposed detection method. Section 6 provides a summary and future research prospects.

2. Three-dimensional double-wing chaotic system

2.1. The proposed system model 1

In recent years, more and more 3D non-autonomous chaotic systems have been proposed and applied to weak signal detection research, showing good detection results and providing new detection ideas for various traditional detection methods based on improved Duffing oscillators. On this basis, a new 3D chaotic system is proposed, named proposed system model 1, and the system model is

$$\begin{cases} \dot{x} = -ax - y + byz, \\ \dot{y} = c(y - xz) + f\sin(wt), \\ \dot{z} = d(-z + xy), \end{cases} \tag{1}$$

where a, b, c, d are positive parameters, x, y, z are state variables, f and w are the amplitude and frequency of the built-in driving force, respectively.

When variables, parameters, and initial conditions (x_0, y_0, z_0) take the following values:

$$\begin{cases} (x_0, y_0, z_0) = (0.1, 0.1, 0.1), \\ (a, b, c, d, f, w) = (35, 2, 1, 1, 2, 1). \end{cases} \tag{2}$$

Figure 1 shows the attractor trajectory and timing diagram of the system. At this time, the phase trajectory looks like a pair of wings, so this system is named 3DDWCS.

By introducing a new dimension, the 3D chaotic system successfully expands the system's attractor from a two-dimensional (2D) phase space to a 3D phase space, which will enable the system to exhibit more complex dynamic behaviors and patterns. For example, a 3D system can generate a more diverse set of trajectories that might not be possible in a 2D space. At the same time, 3D chaotic systems usually show richer nonlinear characteristics, such as period-doubling bifurcations and the appearance of infinitely shrinking attractors, which provide a good foundation for the modeling of complex systems. Next, we will conduct an in-depth study and analysis of the dynamic behavior of 3DDWCS to verify its effectiveness and practicality.

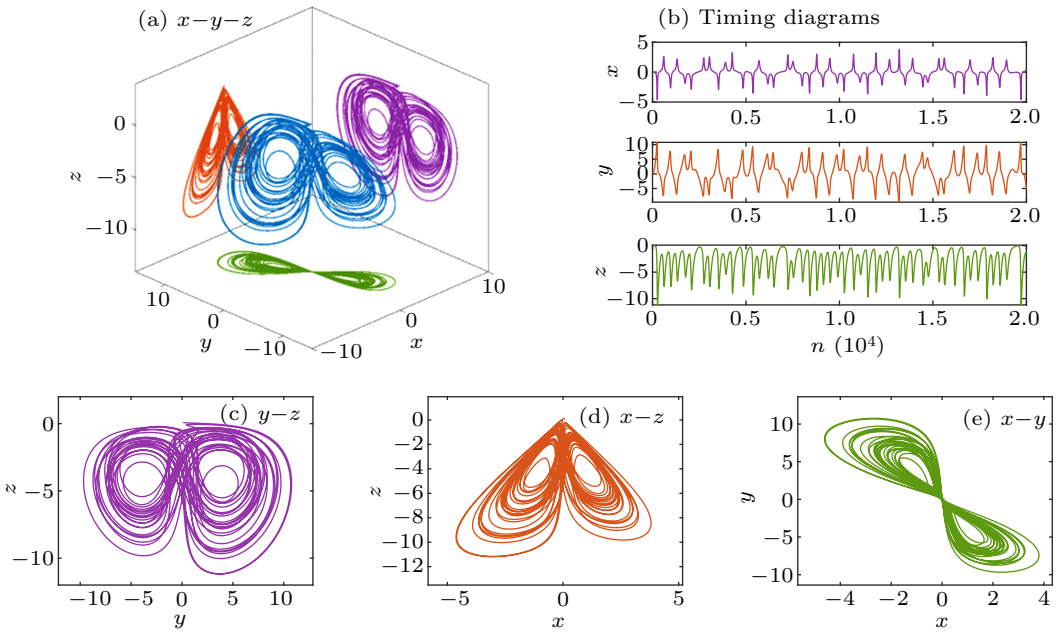


Fig. 1. Attractor trajectories and timing diagrams of 3DDWCS.

2.2. Dissipation

Dissipation reflects the energy loss and stability of a system in its time evolution. Studying dissipation helps to gain a deeper understanding of the long-term behavior of the system.[31] Although 3D chaotic systems show extreme sensitivity to initial conditions, dissipation also plays a smoothing role. Strong dissipation can suppress the impact of small disturbances, causing the system behavior to tend toward a certain stable state. At this time, the dissipation of 3DDWCS is

$$\nabla \cdot V = \frac{\partial \dot{x}}{\partial x} + \frac{\partial \dot{y}}{\partial y} + \frac{\partial \dot{z}}{\partial z} = -a + c - d = -34 < 0. \tag{3}$$

Equation (3) shows that the system is dissipative and the system trajectory will converge to a certain stable state at a speed of exponential $\mathrm{d}V/\mathrm{d}t = \mathrm{e}^{-34t}$.

2.3. Equilibrium and stability

In a chaotic system, the existence of an equilibrium point means that the system can reach a stable state under certain conditions.[32] In mathematical models, an equilibrium point usually refers to the point where the differential equation of the system is zero.

Set the left half of Eq. (1) to 0 and let $t = 0$. The formula for calculating the equilibrium point of 3DDWCS is

$$\begin{cases} 0 = -ax - y + byz, \\ 0 = c(y - xz), \\ 0 = d(-z + xy). \end{cases} \tag{4}$$

Let $J(x,y,z)$ represent the Jacobian matrix of Eq. (1), which is

$$J(x,y,z) = \begin{bmatrix} -a & -1+bz & by \\ -cz & c & -cx \\ dy & dx & -d \end{bmatrix} = \begin{bmatrix} -35 & -1+2z & 2y \\ -z & 1 & -x \\ y & x & -1 \end{bmatrix}. \tag{5}$$

Calculate Eq. (4) to get the equilibrium point of the chaotic system, and then bring the equilibrium point into Eq. (5) to calculate the Jacobian matrix of each equilibrium point. Table 1 lists, in detail, various equilibrium points of 3DDWCS and the corresponding characteristic roots and types.

From Table 1, it can be seen that P_1 is an unstable saddle point, P_2 and P_4 are unstable focus points, P_3 and P_5 are stable focus points. Obviously, the chaotic attractor always moves around focus points P_3 and P_5.

Table 1. The equilibrium points of 3DDWCS and the corresponding characteristic root and type.

Equilibrium points	Characteristic root	Type
$P_1(0,0,0)$	$\lambda_{1,2} = \pm 1$, $\lambda_3 = -35$	Unstable saddle point
$P_2\left(1, \frac{1+\sqrt{281}}{4}, \frac{1+\sqrt{281}}{4}\right)$	$\lambda_{1,2} = 0.1229 \pm 2.0516\mathrm{i}$, $\lambda_3 = -35.2458$	Unstable focus point
$P_3\left(1, \frac{1-\sqrt{281}}{4}, \frac{1-\sqrt{281}}{4}\right)$	$\lambda_{1,2} = -0.0024 \pm 1.9430\mathrm{i}$, $\lambda_3 = -34.9953$	Stable focus point
$P_4\left(-1, -\frac{1+\sqrt{281}}{4}, \frac{1+\sqrt{281}}{4}\right)$	$\lambda_{1,2} = 0.1229 \pm 2.0516\mathrm{i}$, $\lambda_3 = -35.2458$	Unstable focus point
$P_5\left(-1, -\frac{1-\sqrt{281}}{4}, \frac{1-\sqrt{281}}{4}\right)$	$\lambda_{1,2} = -0.0024 \pm 1.9430\mathrm{i}$, $\lambda_3 = -34.9953$	Stable focus point

2.4. Bifurcation diagram

The bifurcation diagram of a chaotic system is an important tool for studying nonlinear dynamics and chaotic behavior. It shows the changes in the system phase trajectory with a certain parameter and can better understand long-term dynamic behavior. Near certain parameter values, the system may show a transition from chaos to periodicity, and these parameter values may be the critical thresholds of the chaotic system. Critical threshold refers to a specific value that leads to a fundamental change in system behavior when system parameters change. Its determination is extremely important for the detection of weak signals.[33] Therefore, the critical threshold can be determined through studying the bifurcation diagram of the chaotic system.

In the process of studying the bifurcation diagram of the five system parameters of 3DDWCS, only one parameter is changed at a time, and the other parameters remain unchanged. See Table 2 for an overview of the simulation parameters and Fig. 2 for the simulation results.

Table 2. Simulation parameters of the bifurcation diagram.

Variable parameters	Constant parameters
$f \in [0,5]$	$(a,b,c,d) = (35,2,1,1)$
$a \in [30,40]$	$(b,c,d,f) = (2,1,1,2.6)$
$b \in [0,5]$	$(a,c,d,f) = (35,1,1,2.6)$
$c \in [0,5]$	$(a,b,d,f) = (35,2,1,2.6)$
$d \in [0,5]$	$(a,b,c,f) = (35,2,1,2.6)$

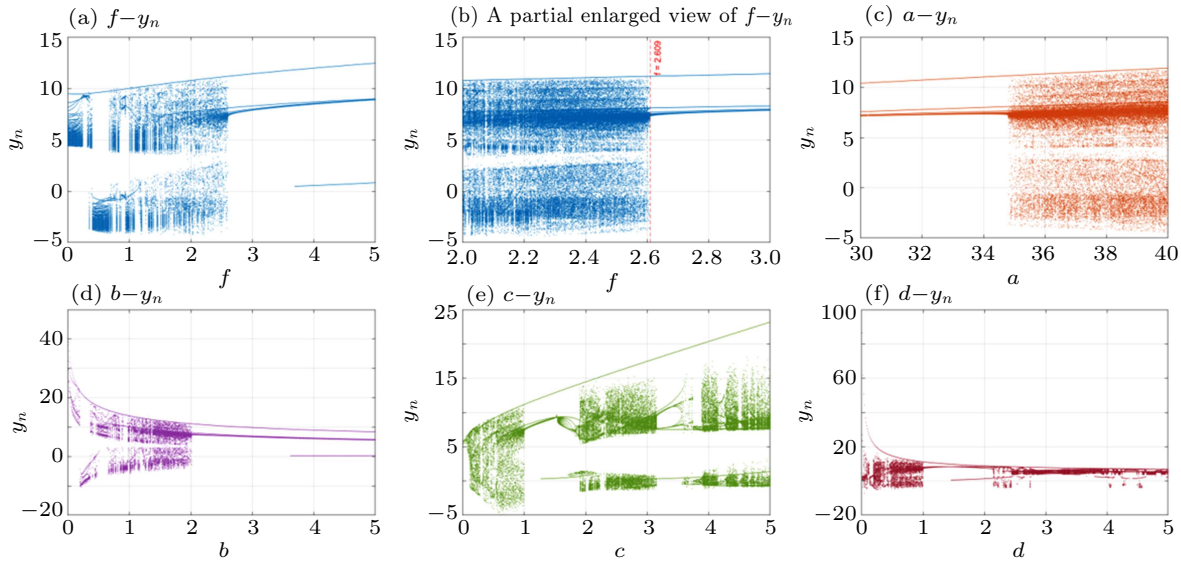


Fig. 2. Bifurcation diagrams for various parameters.

Figures 2(a)–2(f) show the bifurcation diagram corresponding to each parameter. According to Fig. 2(a), the critical threshold f_1 of the chaotic system ranges from 2 to 3. Therefore, the bifurcation diagram of f–y_n when $f \in (2,3)$ is plotted with a step size of 0.001, see Fig. 2(b), and $f_1 = 2.609$ can be obtained. According to Figs. 2(d)–2(f), 2, 1, 1 are also critical states of functions b–y_n, c–y_n, and d–y_n, respectively.

2.5. Lyapunov exponent

The Lyapunov exponent quantifies the sensitivity of a system to perturbations in its initial conditions, indicating how a small initial perturbation grows over time.[34] Through the Lyapunov exponent, researchers can classify the system into different states such as stable, borderline stable, or chaotic, which provides a basis for further analysis and also provides a specific measurement for the dynamic stability and sensitivity of the system. In practical applications, the combination of bifurcation diagrams and Lyapunov exponents can provide a more overall understanding of the behavioral characteristics of complex nonlinear systems.

The Lyapunov exponent expression of a 3D chaotic system is

$$[\lambda_1,\lambda_2,\lambda_3] = \lim_{t\to\infty}\frac{1}{t}\left[\ln\left|\frac{\partial x(t)}{\partial x(0)}\right|,\ln\left|\frac{\partial y(t)}{\partial y(0)}\right|,\ln\left|\frac{\partial z(t)}{\partial z(0)}\right|\right]. \quad (6)$$

In the process of studying the Lyapunov exponent of the five system parameters of 3DDWCS, only one parameter is changed at a time, and the other parameters remain unchanged. See Table 2 for an overview of the simulation parameters and Fig. 3 for the simulation results.

Figures 3(a)–3(f) show the Lyapunov exponent corresponding to each parameter. According to Fig. 3(a), the critical threshold f_1 of the chaotic system ranges from 2 to 3. Therefore, the Lyapunov exponent of $f-y_n$ when $f \in (2,3)$ is plotted with a step size of 0.001, see Fig. 3(b), $f_1 = 2.609$ can be obtained. According to Figs. 3(d)–3(f), 2, 1, 1 are also critical states of functions $b-Ly$, $c-Ly$, $d-Ly$, respectively. When the simulation parameters are the same, the place where chaos occurs represented by the bifurcation diagram of 3DDWCS is consistent with the Lyapunov exponent.

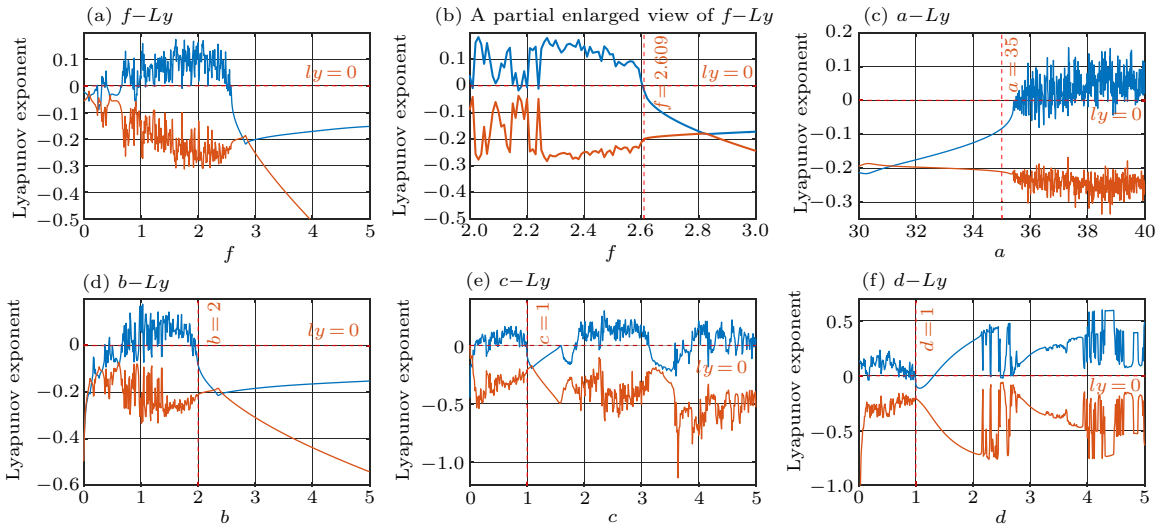


Fig. 3. Lyapunov exponent for various parameters.

2.6. Initial condition sensitivity

Based on the parameters in Eq. (2), we apply perturbations of 0.001 and 0.00001 to the chaotic system's variable y and observe the changes in the system's timing diagram. Figure 4 shows the evolution of the time series. It demonstrates that the 3DDWCS is extremely sensitive to initial conditions.

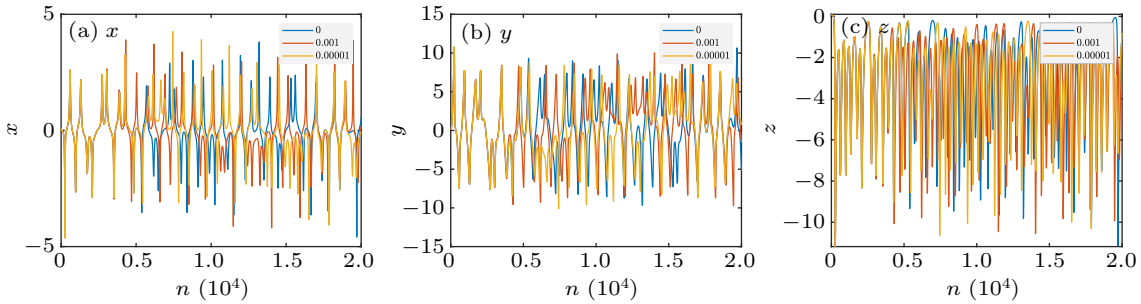


Fig. 4. Initial condition sensitivity of sequences x, y, z.

2.7. Power spectrum

Chaotic signals generated by the iteration of chaotic systems are highly random and complex. The wide frequency distribution, uniform energy distribution, and complex dynamic behavior of the chaotic signal in the generation process together lead to the smoothness of the power spectrum of the chaotic system. This characteristic is one of the typical signs of the chaotic system. When the system takes the value shown in Eq. (2), Figs. 5(a)–5(c) show the power spectra of three state variables x, y, z, respectively. The simulation results show that the variables of 3DDWCS have an almost smooth power spectrum. Therefore, 3DDWCS has typical chaotic characteristics.

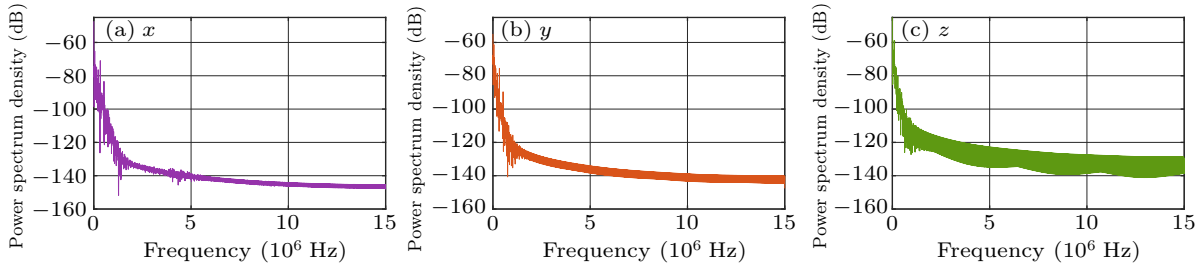


Fig. 5. Power spectra of variables.

2.8. Simulink dynamic simulation

Simulink is a graphical tool for modeling, simulation, and analysis of dynamic systems, and is widely used in control systems, signal processing, and other fields. According to Eqs. (1) and (2), a simulation model of 3DDWCS is built and run. Figure 6 is the simulation model, and Fig. 7 is the simulation results. Figures 7(a)–7(c) are the three plane phase diagrams of 3DDWCS at this time, and Figs. 7(d)–7(e) are the timing diagrams at this time. The results are basically consistent with Fig. 1.

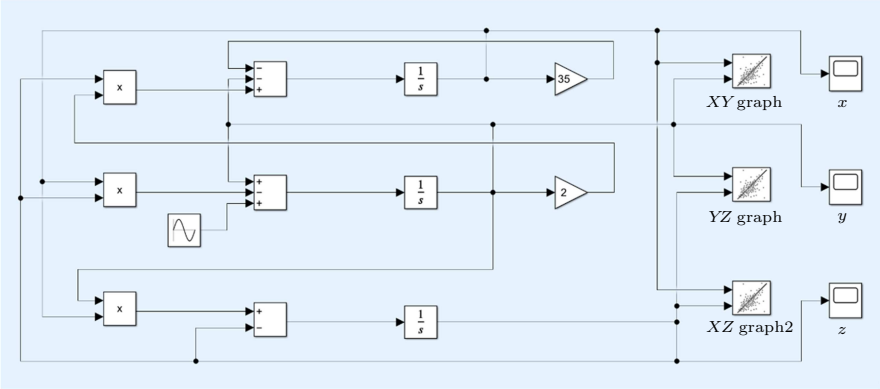


Fig. 6. The simulation model of 3DDWCS.

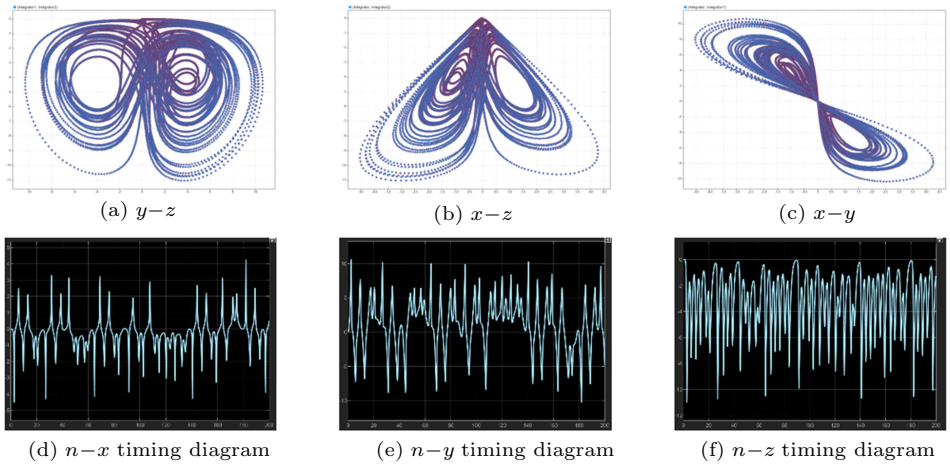


Fig. 7. The simulation results.

2.9. System dynamics and performance analysis

It can be seen from the above analysis that 3DDWCS has chaotic characteristics and can detect weak signals in theory. Next, the change of 3DDWCS with the parameter f will be emphatically analyzed, and the state of 3DDWCS will be determined through the state of the y–z phase diagram. The phase trajectory of 3DDWCS is plotted based on Figs. 2(a), 2(b) and 3(a), 3(b) as shown in Fig. 8.

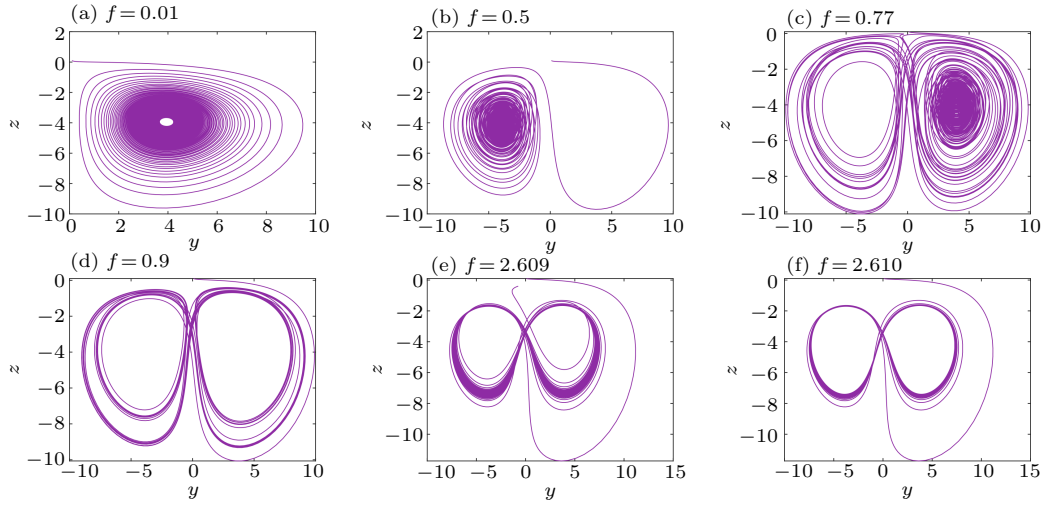


Fig. 8. Evolution process of the 3DDWCS phase trajectory when $f \in [0,5]$.

As can be seen from Fig. 8, the evolution process of the 3DDWCS phase trajectory has roughly three stages: chaotic attractor, chaotic double wings, and periodic double wings, among which (a) is the first stage, (b)–(e) are the second stage, and (f) is the third stage. The phenomenon of spiral chaos appears in Figs. 8(a)–8(c). At the same time, Fig. 8(e) is the

phase diagram when the system is in a critical chaotic state, and Fig. 8(f) is the phase diagram when the system is in a large-scale periodic state. It is verified that $f = 2.609$ is the critical threshold of 3DDWCS.

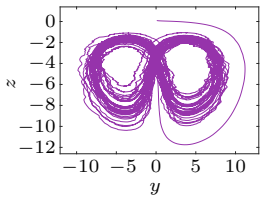
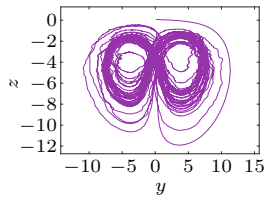
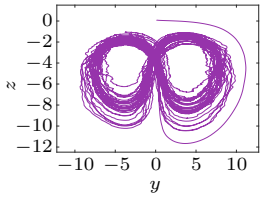
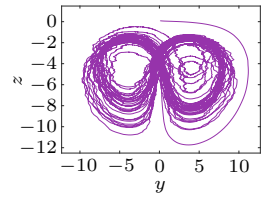
Let $P = f_1 \sin(wt) + n(t)$ be the signal to be measured, $n(t)$ be the noise, adjust 3DDWCS to the critical state, that is, $f = 2.609$, and then input P into the detection system to obtain

$$\begin{cases} \dot{x} = -35x - y + 2yz, \\ \dot{y} = y - xz + 2.609\sin(wt) + P, \\ \dot{z} = -z + xy. \end{cases} \tag{7}$$

When $n(t)$ is Gaussian white noise with a mean of 0 and an intensity of δ, let the minimum f_1 that 3DDWCS can detect be $f_{1,\min}$ and substitute it into Eq. (8) to calculate the SNR threshold of the system.[35] The results of the performance analysis of 3DDWCS under different noise intensities are shown in Table 3.

$$\mathrm{SNR} = 10\lg\left(\frac{f_{1,\min}^2}{2\delta^2}\right). \tag{8}$$

Table 3. Results of the 3DDWCS performance analysis under different noise intensities.

δ	Amplitude detection result		SNR (dB)
0.1			−67.44
	$f_1 = 0.00006$	$f_1 = 0.00005$	
0.05			−64.94
	$f_1 = 0.00004$	$f_1 = 0.00003$	

As shown in Table 3, when $\delta = 0.1$, $f_{1,\min} = 0.00006$ and SNR $= -67.44$ dB; when $\delta = 0.05$, $f_{1,\min} = 0.00004$ and SNR $= -64.94$ dB. In general, the detection effect of 3DDWCS is good, and the SNR threshold is low. However, it can be seen from the y–z phase diagram of Table 3 $\delta = 0.1$, $f_1 = 0.0001$ and $\delta = 0.05$, $f_1 = 0.00004$ that although the system is in a periodic state, the phase trajectory is loose and rough, indicating that the system's anti-noise performance is general. Therefore, we introduce fractional-order calculus into 3DDWCS to improve the anti-noise performance of the detection system.

3. Fractional-order three-dimensional double-wing chaotic systems

The application of fractional-order calculus in chaotic systems shows unique advantages, especially in the accuracy of complex system modeling, the richness of dynamic behavior, and the superiority of system performance. Taking advantage of this unique advantage, the ability of the chaotic system to detect weak signals can be significantly improved, which not only improves the accuracy of signal capture and feature analysis but also enables the chaotic system to work effectively in complex and dynamic environments, providing reliable support for practical applications.

3.1. The proposed system model 2

The fractional-order derivative is introduced into Eq. (1), and the fractional-order 3D double-wing chaotic system (FO3DDWCS) is obtained, which is named proposed system model 2. The system model is

$$\begin{cases} D_t^q x = w(-ax - y + byz), \\ D_t^q y = w\left[c(y - xz) + f\sin(wt)\right], \\ D_t^q z = w\left[d(-z + xy)\right], \end{cases} \tag{9}$$

where q is the order.

The parameter values of Eq. (9) are

$$\begin{cases} (a,b,c,d) = (35,2,1,1), \\ (x_0,y_0,z_0) = (0.1,0.1,0.1). \end{cases} \tag{10}$$

The numerical approximate solution of FO3DDWCS is calculated using the Adams–Bashforth–Moulton prediction-correction method based on the Caputo definition and is used to plot the phase diagram of FO3DDWCS. The fractional-order Adams method introduced in Ref. [36] is one of the most effective prediction-correction methods and is widely used to solve fractional-order differential equations involving Caputo-type fractional-order derivatives.

3.2. Selection of fractional order and determination of critical thresholds

The integer-order chaotic system can be understood as a special case of fractional-order chaotic systems when the or-

der is an integer. Except for the order of the system, the influence of other parameters in a fractional chaotic system is similar to that in the integer chaotic system. Based on this, the research focus will be on the influence of fractional order on 3DDWCS. Therefore, the SE complexity diagram and fluctuation dispersion entropy (FDE) diagram varying with parameter q are used for analysis. The parameters of FO3DDWCS take Eq. (9), $f = 2.971$ and $w = 1$, and the results are shown in Fig. 9.

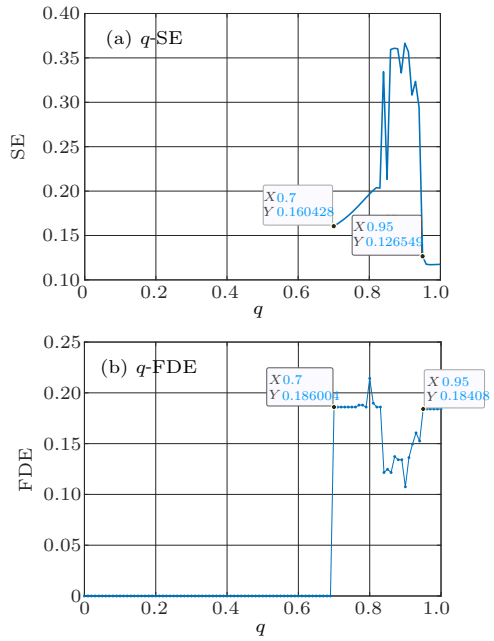


Fig. 9. SE complexity diagram and FDE diagram of FO3DDWCS varying with parameter q.

As can be seen from Fig. 9, when $q > 0.7$, FO3DDWCS has higher entropy complexity, which means it has richer dynamic behavior. Next, based on Eq. (9), the step size is 0.01. Taking $q = 0.95$ and $q = 0.99$ as an example, the bifurcation diagrams f–y_n under different orders are compared. The simulation results are shown in Fig. 10, where (a) is the bifurcation diagram when $q = 0.95$, (b) is a local intercept diagram of (a) when $f \in (2,4)$, (c) is the bifurcation diagram when $q = 0.99$, and (d) is a local intercept diagram of (c) when $f \in (2,4)$.

It can be observed from Figs. 10(a) and 10(c) that the bifurcation diagrams when $q = 0.95$ and $q = 0.99$ are similar. Therefore, take local intercept diagrams respectively when $f \in (2,4)$, as shown in Figs. 10(b) and 10(d). It can be observed that the convergence speed of $q = 0.95$ is greater than that of $q = 0.99$ near the critical threshold, which will make the phase trajectory contrast when the chaotic system changes from a chaotic state to a large-scale periodic state at the critical threshold more obvious, and the critical threshold that can be selected is more accurate, which lays a good foundation for the detection of weak signals. Therefore, this paper selects the detection system when $q = 0.95$ for detection experiments.

The critical threshold f_1 of the system should be determined before using FO3DDWCS for weak signal detection. It can be seen from Figs. 10(a) and 10(b) that $f_1 \in (2.7, 3.3)$, so the step size is 0.001 and the bifurcation diagram when $f \in [2.7, 3.3]$ is drawn, as shown in Fig. 11, and the critical threshold can be obtained $f_1 = 2.971$.

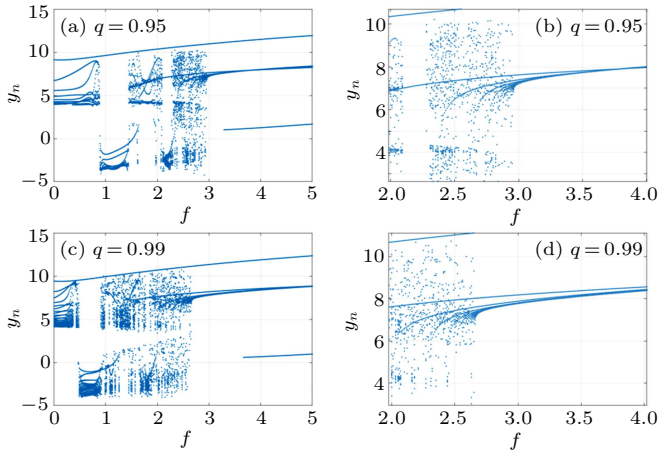


Fig. 10. Bifurcation diagrams for parameter f.

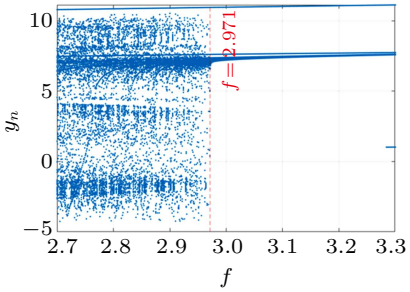


Fig. 11. Bifurcation diagrams for parameter f when the step size is 0.001.

3.3. System dynamics and performance analysis

The phase trajectory of FO3DDWCS is drawn according to Fig. 10(a), as shown in Fig. 12. As can be seen from Fig. 12, the evolution process of the FO3DDWCS phase trajectory has roughly three stages: chaotic attractor, chaotic double wings, and periodic double wings, among which (a) is the first stage, (b), (c), and (e) are the second stage, (g) is the third stage, (d) is the 3D phase diagram of (e), and (f) is the 3D phase diagram of (g). The phenomenon of spiral chaos appears in Fig. 12(a). At the same time, Figs. 12(d) and 12(e) are phase diagrams when the system is in a critical state, and Figs. 12(f) and 12(g) are phase diagrams when the system is in a large-scale periodic state. It is verified that $f = 2.971$ is the critical threshold of FO3DDWCS. Its dynamic behavior is similar to that of 3DDWCS, both of which have three stages. The comparison of the state changes of the two systems when $f \in [0,5]$ is shown in Table 4.

Table 4. Comparison of state changes between 3DDWCS and FO3DDWCS in $f \in [0,5]$.

System status	f	
	3DDWCS	FO3DDWCS
Phase 1	0–0.33	0–0.88
Phase 2	0.34–2.609	0.89–2.971
Phase 3	2.610–5	2.972–5

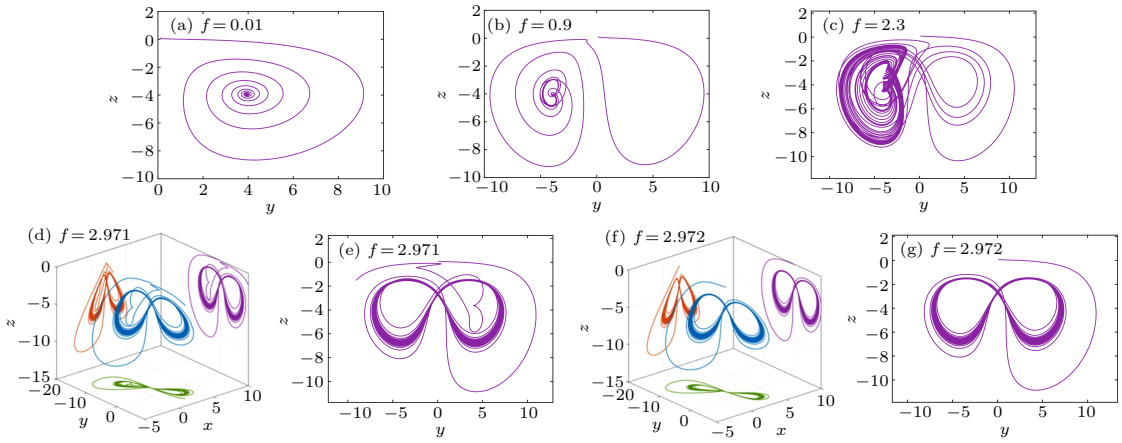
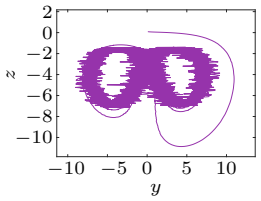
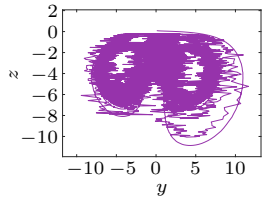
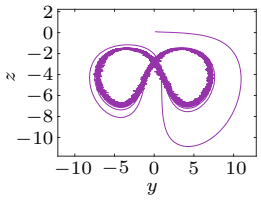
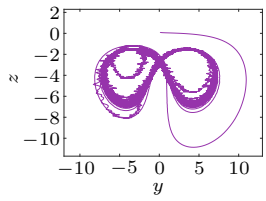


Fig. 12. Evolution process of the FO3DDWCS phase trajectory when $f \in [0,5]$.

Table 5. The performance analysis results of FO3DDWCS under different noise intensities.

δ	Amplitude detection result		SNR (dB)
0.1			−124.94
	$f_1 = 0.8\times10^{-7}$	$f_1 = 0.7\times10^{-7}$	
0.05			−116.98
	$f_1 = 0.1\times10^{-6}$	$f_1 = 0.9\times10^{-7}$	

Next, the performance of FO3DDWCS is analyzed. The system is adjusted to the critical state, which is $f = 2.971$, and the signal to be measured $P = f_1\sin(wt) + n(t)$ is input into the detection system to obtain

$$\begin{cases} D_t^{0.95}x = w(-35x - y + 2yz), \\ D_t^{0.95}y = w\left[y - xz + 2.971\sin(wt) + P\right], \\ D_t^{0.95}z = w(-z + xy). \end{cases} \tag{11}$$

When $n(t)$ is a Gaussian white noise with a mean of 0 and an intensity of δ, the minimum f_1 that FO3DDWCS can detect is $f_{1,\min}$. Substitute it into Eq. (8) to calculate the SNR threshold of the system. Table 5 shows the performance analysis results of FO3DDWCS under different noise intensities.

As shown in Table 5, when $\delta = 0.1$, $f_{1,\min} = 0.8\times10^{-7}$ and SNR $= -124.94$ dB; when $\delta = 0.05$, $f_{1,\min} = 0.1\times10^{-6}$ and SNR $= -116.98$ dB. It can be seen that FO3DDWCS has an excellent detection effect and can detect weak signals under ultra-low SNR thresholds. At the same time, it can be seen from the y–z phase diagrams of Table 5 $\delta = 0.1$, $f_1 = 0.8\times10^{-7}$ and $\delta = 0.05$, $f_1 = 0.1\times10^{-6}$ that at this time the system exhibits a periodic state, and the phase trajectory is relatively smooth and compact, indicating that the system's anti-noise performance has been greatly improved compared with 3DDWCS.

The detection performances of FODCDS, FODVP, FOHOD-VPO, 3D chaotic system 1, 3D chaotic system 2, 3DDWCS and FO3DDWCS are compared, and the detection performance results of the seven chaotic systems are shown in Table 6. The first three detection systems are fractional-order chaotic systems based on the improvement of the Duffing oscillator, and the fourth and fifth detection systems are 3D chaotic systems proposed in recent years that introduce a new variable z.

It can be seen from Table 6 that, under the background of Gaussian white noise with an intensity of 0.05, the minimum detectable SNR thresholds of the proposed 3DDWCS and FO3DDWCS are −64.94 dB and −116.98 dB, respectively. Under the background of Gaussian white noise with an intensity of 0.1, the minimum detectable SNR thresholds of the proposed 3DDWCS and FO3DDWCS are −67.44 dB and −124.94 dB, respectively. It can be concluded that FO3DDWCS has a lower SNR threshold than both the

Table 6. The detection performance results of the seven chaotic systems.

Detection model	Noise intensity			
	0.05		0.1	
	SNR (dB)	$f_{1,\min}$	SNR (dB)	$f_{1,\min}$
FODCDS[11]	n.a	n.a	–43.01	0.001
FODVP[29]	n.a	n.a	–69.03	0.00005
FOHOD-VPO[30]	n.a	n.a	–70.97	0.00004
3D chaotic system 1[14]	–57	0.0001	–63	0.0001
3D chaotic system 2[15]	–51	0.0002	–53	0.0003
3DDWCS	–64.94	0.00004	–67.44	0.00006
FO3DDWCS	–116.98	0.1×10^{-6}	–124.94	0.8×10^{-7}

Note: "n.a" represents that performance data is unavailable for systems.

integer-order 3D chaotic system and the fractional-order chaotic system improved based on the Duffing oscillator, and can detect weak signals under ultra-low SNR threshold with excellent detection effect.

4. Weak signal detection

The phase trajectory is the path of the state of a dynamic system in the phase space, representing the evolution of the state variables over time. For chaotic systems, the phase trajectory may show complex and irregular behavior. External signals such as periodic signals affect the state of the system. When the external signal contains specific frequency components, these frequencies will affect the phase trajectory in a specific way. Therefore, the chaotic system can effectively detect the signal frequency by analyzing the phase trajectory.

4.1. The proposed detection method

With the continuous progress of ship stealth technology, the sound level of SRN is becoming increasingly weak, which makes it difficult for the SNR threshold of the existing detection system to meet the detection requirements.[37] In order to realize the detection of weak signals under ultra-low SNR threshold, a weak signal detection method based on FO3DDWCS is proposed and applied to the detection of SRN. The basic steps of this method to detect signal frequency are given as follows.

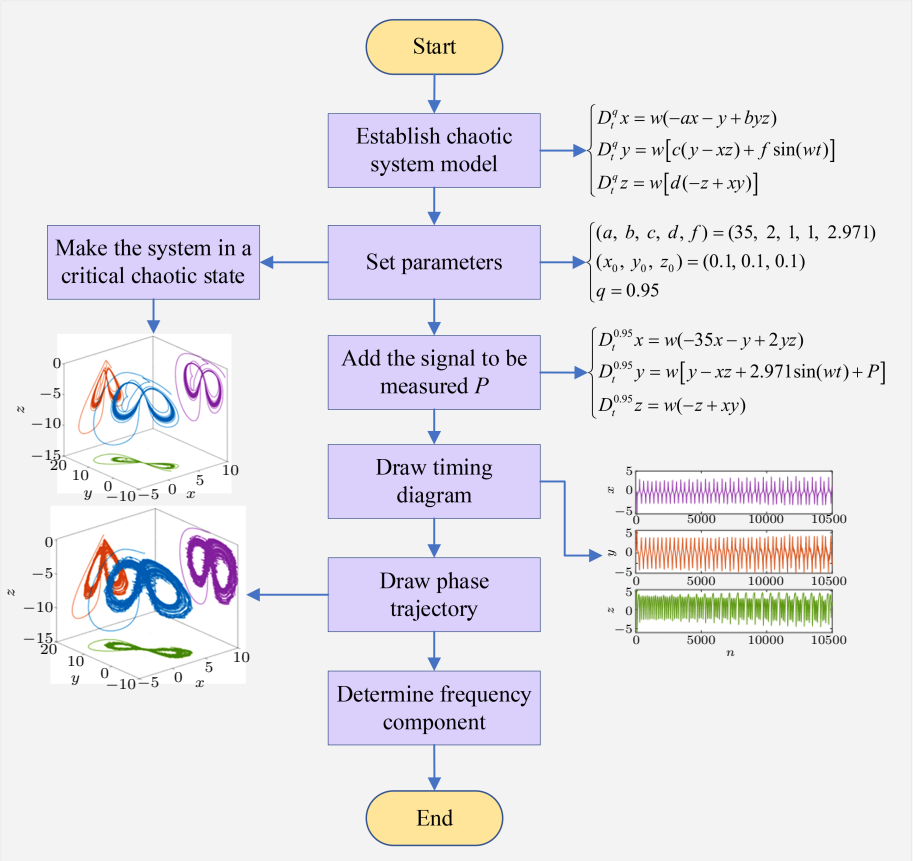


Fig. 13. A flow chart of the proposed detection method.

Step 1: Establish a chaotic system model, as shown in Eq. (9), and obtain its dynamic behavior through simulation experiments.

Step 2: Set parameters, as shown in Eq. (10). Define system parameters such as initial conditions, driving frequency, etc. to ensure that the system is in a critical chaotic state.

Step 3: Add the signal to be measured, which is a periodic signal containing unknown frequency components, into the chaotic system, as shown in Eq. (11).

Step 4: Draw timing diagram. The system state variables x, y and z are recorded through simulation experiments, and the recorded data are organized to form a time series diagram.

Step 5: Draw phase trajectory. By plotting the trajectory of state variables in the phase space, the phase trajectory of the system can be observed.

Step 6: Determine frequency component. When the phase trajectory in Figs. 12(d) and 12(e) changes from a chaotic state to a periodic state and the signal in the timing diagram changes from a disordered signal to an ordered signal, the periodic signal frequency in the signal to be measured can be detected, that is, it is equal to the frequency of the chaotic system.

Based on the above steps, the flow chart of the proposed detection method is shown in Fig. 13. The general flow chart of the article is shown in Appendix A.

4.2. Detection experiment

Next, based on the proposed detection method, detection experiments are carried out on the basis of the detection system, see Eq. (11). The analog signal, SRN, and marine biological signal (MBS) are input into the detection system FO3DDWCS, respectively, and the changes in the system phase diagram and timing diagram are observed.

4.2.1. Analog signal detection experiment

A multi-spectrum periodic signal consists of multiple frequency components, which can be expressed as the superposition of multiple sine waves. This diversity can effectively simulate various signal characteristics that may be encountered in practical applications. Multiple signals of different waveforms can be superimposed on the same frequency. If the target being detected (sinusoidal signal) is polluted by an irrelevant signal, the signal will be distorted. Therefore, the sine signal and the square wave can be combined to form a distortion signal, and the ability to detect the distortion signal can be evaluated by injecting the distortion signal into the detection system.

However, actual signals are often accompanied by noise. Therefore, adding noise to multi-spectrum periodic signals and distorted signals respectively can more realistically simulate the signal environment in actual applications, making the experimental results more realistic and helpful in verifying the practicality of chaotic systems in complex environments. Using the noisy multi-spectrum periodic signal and the noisy distorted signal, the analog signal detection experiment is carried out respectively. The specific expressions are shown in Table 7, where there is Gaussian white noise with a mean of 0 and an intensity of 0.05. The built-in driving force frequency of the detection system is set to 2 and 3 respectively. The detection results of the analog signal are shown in Fig. 14.

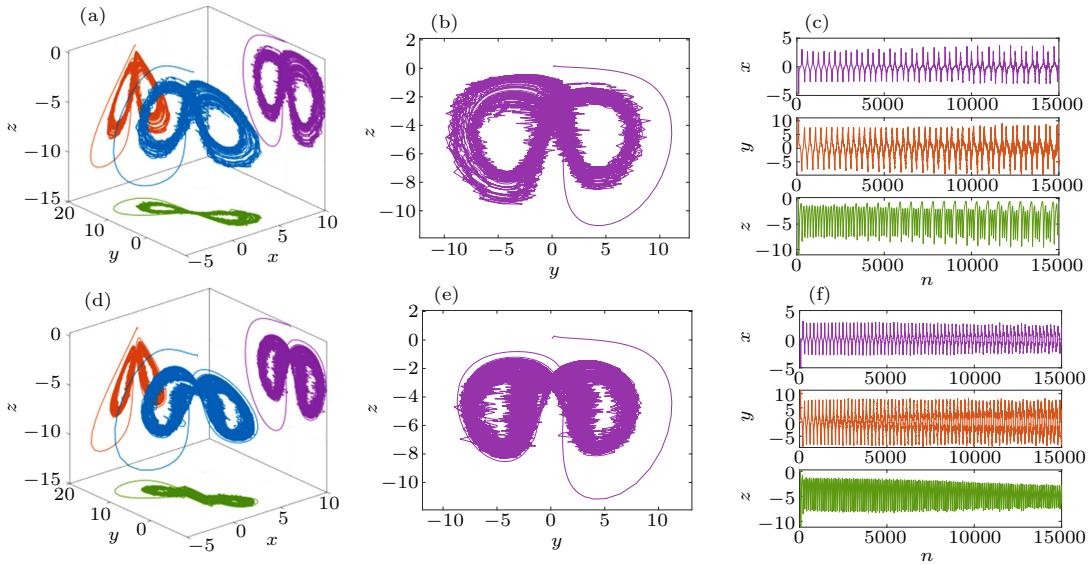


Fig. 14. Analog signal detection results: (a), (b), (c) noisy multi-spectrum periodic signal; (d), (e), (f) noisy distorted signal.

Table 7. Analog signal.

Analog signal	Signal composition	Built-in driving frequency w
Noisy multi-spectrum periodic signal	$P = 0.01\,[\sin(1t) + \sin(2t) + \sin(3t)] + n(t)$	2
Noisy distorted signal	$P = 0.01\,[\sin(3t) + \mathrm{square}(3t)] + n(t)$	3

Figures 14(a)–14(c) show the detection results of the noisy multi-spectrum periodic signal. At this time, the phase diagram shows a periodic state, and the signal in the timing diagram is an ordered signal, indicating that the detection system Eq. (11) detects a periodic signal with a frequency of 2 in the noisy multi-spectrum periodic signal. Figures 14(d)–14(f) show the detection results of the noisy distorted signal. At this time, the burrs on the y–z plane phase diagram are more serious, but it can still be seen from the 3D phase diagram that the system is in a periodic state, and the signal in the timing diagram is an ordered signal, indicating that the detection system Eq. (11) detects a periodic signal with a frequency of 3 in the noisy distorted signal. The effectiveness of the proposed detection method is verified.

4.2.2. Ship radiated noise detection experiment

The proposed detection method is tested by using SRN, which is nonlinear and unsteady.[38,39] The data of four merchant ship categories come from https://github.com/irfankamboh/DeepShip. The sampling frequency of the data is 32 KHz. A set of data from passenger ships, tugboats, and tankers are selected respectively, and resampled at 1 kHz and 15000 sampling point fragments are intercepted, named E1, E2, and E3 respectively. The signals are normalized and tested as the signals are measured. The time domain waveform and power spectrum of the sampled data are shown in Fig. 15, where the first column and the second column are the time domain waveform and the power spectrum of E1, E2, and E3 respectively. The frequencies of E1, E2, and E3 are 2.57143 Hz, 2.42857 Hz, and 2 Hz, respectively.

The SRN E1, E2, and E3 are respectively input into the detection system Eq. (11), and the detection results are reflected by the phase trajectory and timing diagram of the system. If the system state becomes a stable periodic state, it means that the signal to be measured contains a periodic signal. The detection results are shown in Fig. 16, where Figs. 16(a)–16(c) are the detection results of E1, Figs. 16(d)–16(f) are the detection results of E2, and Figs. 16(g)–16(i) are the detection results of E3.

As can be seen from Fig. 16, all timing diagrams are sequential signals, and all phase trajectories change from the critical threshold state in Figs. 12(d) and 12(e) to the large-scale periodic state, which proves that the detection system successfully detects the frequency of E1 as 2.57143 Hz, the frequency of E2 as 2.42857 Hz, and the frequency of E3 as 2 Hz. The effectiveness of the proposed detection method is verified. Compared with the large-scale periodic states in Figs. 12(f) and 12(g), the periphery of the phase trajectory in Fig. 16 is obviously thickened and has obvious burrs. This is due to the influence of various noises in the SRN and is a normal phenomenon.

4.2.3. Marine biological signal detection experiment

In order to verify the universality of the proposed detection method, this study used this method to verify the MBS. The audio data come from the website http://www.whoi.edu/watkinssounds. Select a set of data of Bottlenose Dolphin and Harp Seal respectively, resample at 1 kHz and intercept 15000 sampling points, named F1 and F2, respectively. Figure 17 shows the time domain waveform and power spectrum of the sampled data, where the frequencies of F1 and F2 are 0.714286 Hz and 3 Hz, respectively. The detection results are shown in Fig. 18.

As shown in Fig. 18, the phase diagram of the system is periodic, which proves that the proposed detection system successfully detects the F1 frequency of 0.714286 Hz and the F2 frequency of 3 Hz, and verifies the universality of the proposed detection method.

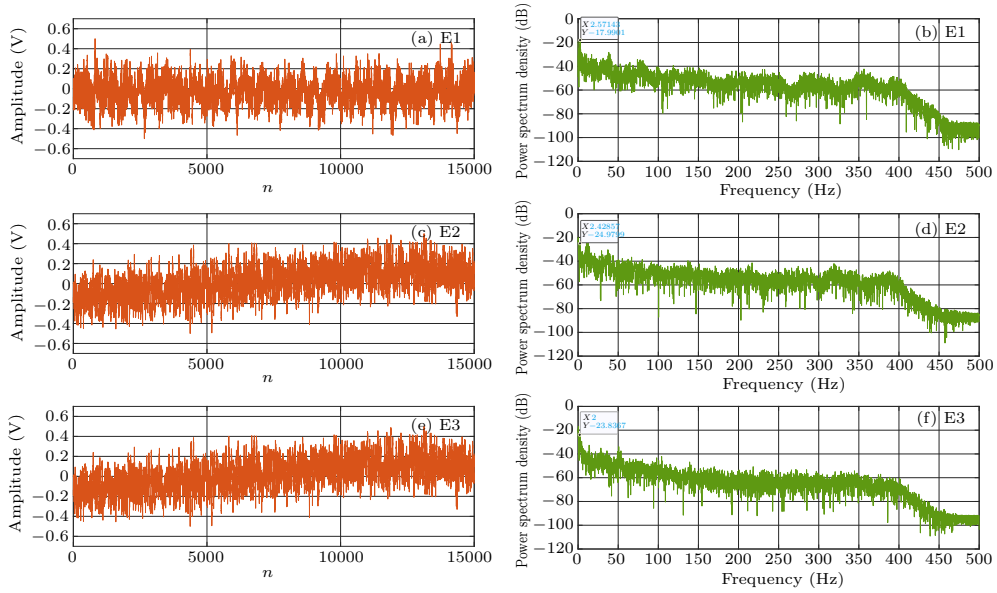


Fig. 15. Time domain waveform and power spectrum of SNR.

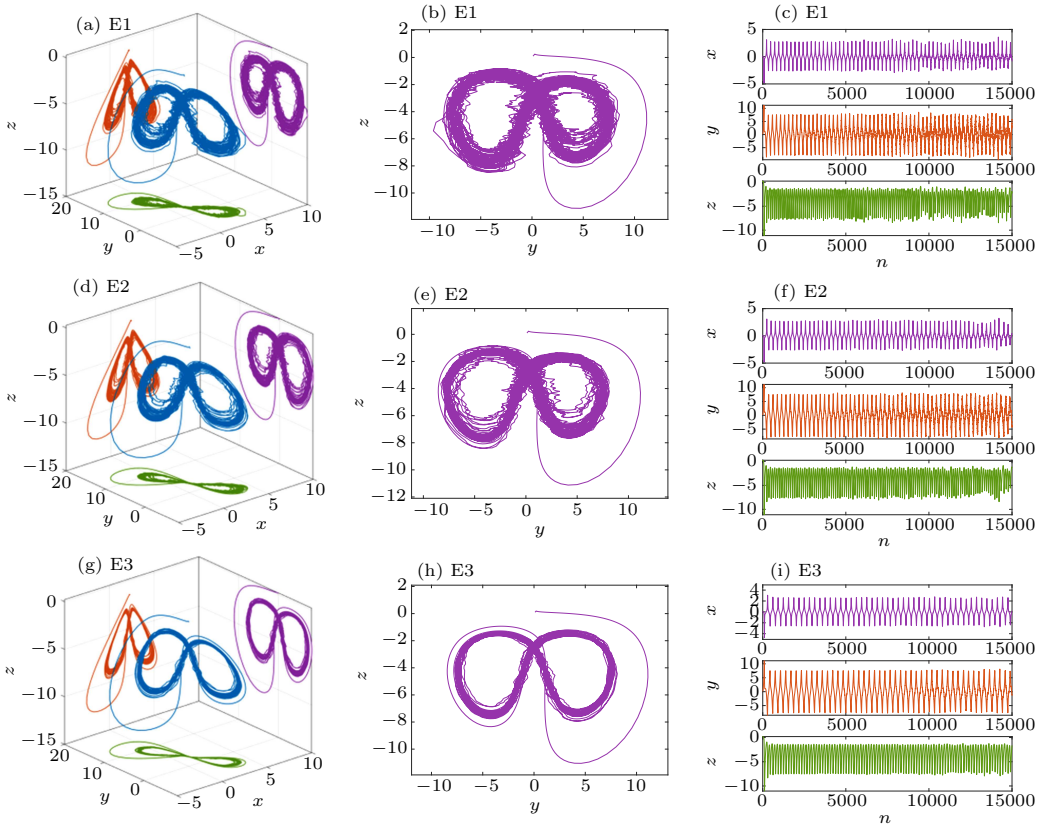


Fig. 16. SNR detection results.

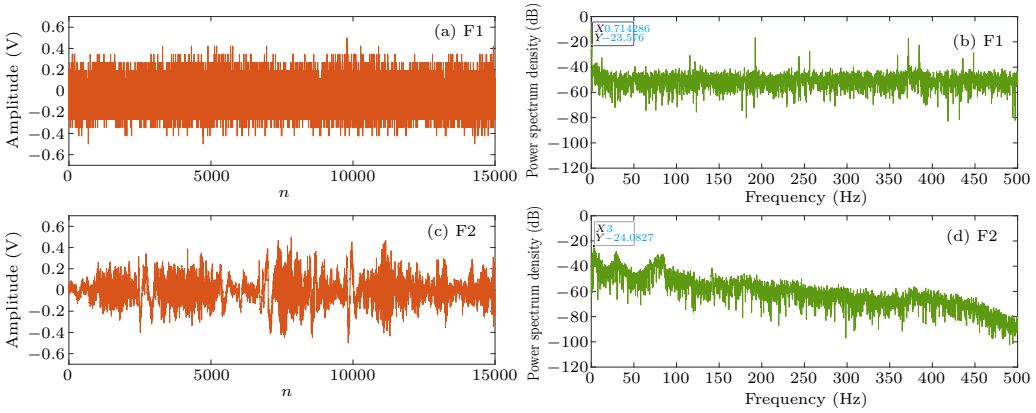


Fig. 17. The time domain waveform and power spectrum of MBS.

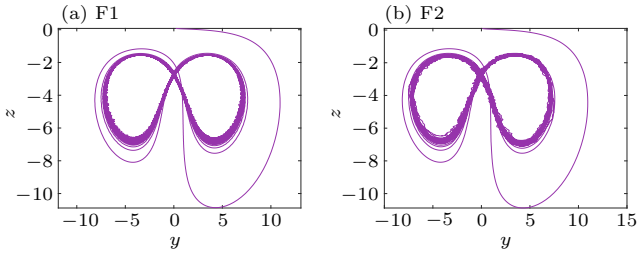


Fig. 18. The detection results of MBS.

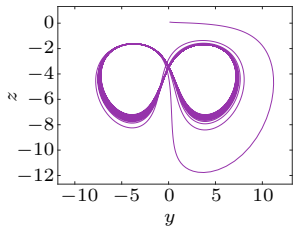
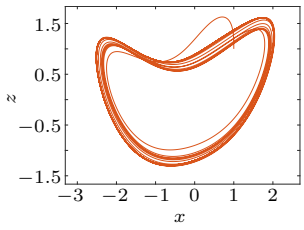
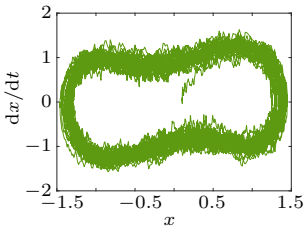
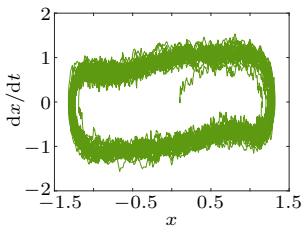
4.2.4. Comparison of detection methods

At the same time, in order to better reflect the detection situation of FO3DDWCS in the application, the SRN E3 is input into the detection system 3DDWCS, 3DCS1, FODVP, and FOHOD-VPO, respectively. The detection results are shown in Table 8.

As can be seen from Table 8, all systems can successfully detect the periodic signal in E3. However, by comparing the detection results of FO3DDWCS in Fig. 16(h) with the phase diagrams of integer-order chaotic systems 3DDWCS and 3DCS1, it can be found that the phase diagram of the integer-order system is relatively smooth, while the phase diagram of the fractional-order chaotic system FO3DDWCS shows more details and glitches. This phenomenon shows that the fractional-order chaotic system is more sensitive to noise, can better capture subtle changes in the signal, and has higher detection accuracy. In contrast, the phase diagrams of other fractional-order chaotic systems FODVP and FOHOD-VPO are rougher and have more glitches, indicating that their

anti-noise performance is weaker. In addition, combined with the SNR data of each system in Table 6, FO3DDWCS has the lowest SNR, which further verifies its superior performance in weak signal detection. In summary, the proposed FO3DDWCS system shows significant advantages in both anti-noise performance and detection accuracy.

Table 8. Detection results of each system after adding SRN E3.

	Phase diagram	
Integer-order chaotic system		
	3DDWCS	3D chaotic system 1[14]
Fractional-order chaotic system		
	FODVP[29]	FOHOD-VPO[30]

5. Discussion

The proposed detection method can detect the existence of the signal to be measured, but it still has some limitations:

(1) By introducing a new dimension, the attractor of the system is successfully extended from the 2D phase space to the 3D phase space. The 3D chaotic system can generate more diverse trajectories, which may not be realized in the 2D space. However, the specific characteristics of the FO3DDWCS changing from chaos to order at the critical threshold are not well understood. In the future, the detailed changes of the 3D phase trajectory near the critical threshold will be studied.

(2) The detection of SRN can only be based on the power spectrum diagram of the signal to determine the possible frequency components of the signal, and the frequency of the signal cannot be accurately determined through the system. Subsequent work will use the frequency sweep method to detect signals of unknown frequencies.

6. Conclusions

In order to detect weak signals under an ultra-low SNR threshold, a weak signal detection method based on FO3DDWCS is proposed and applied to the detection of SRN. The main conclusions of this paper are summarized as follows.

(1) A 3DDWCS with a sine term is proposed. The nonlinear characteristics of the 3DDWCS, such as bifurcation, Lyapunov exponent, and equilibrium point, are analyzed in detail. A Simulink simulation model of 3DDWCS is established and run. It is proven that the 3DDWCS can be used for the detection of weak signals with good detection effect.

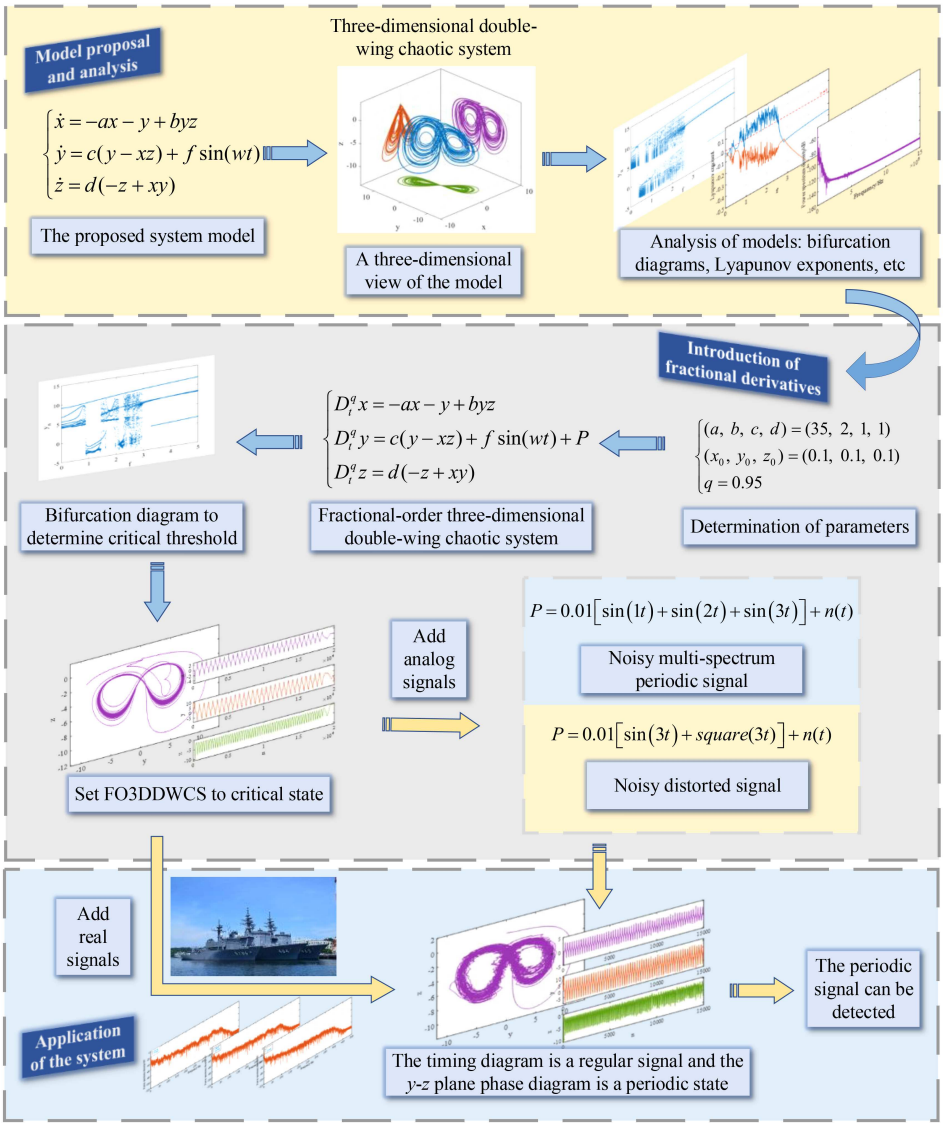
(2) FO3DDWCS is proposed. Fractional calculus is introduced into 3DDWCS, and the selection of the fractional order is discussed. The critical threshold of the system is determined through the bifurcation diagram and then verified based on the phase trajectory.

(3) In the performance analysis experiment, the output SNR threshold of 3DDWCS is relatively low, which is -67.44 dB. The performance of FO3DDWCS considering fractional-order derivatives is better, with an SNR threshold of -124.94 dB, achieving signal detection under an ultra-low SNR threshold. The proposed FO3DDWCS is significantly better than the integer-order 3D chaotic system and the fractional-order chaotic system based on the Duffing oscillator in terms of noise resistance and has an excellent detection effect.

(4) A weak signal detection method based on FO3DDWCS is proposed and successfully applied to the detection of multi-line spectrum periodic signals, distorted signals, SRN, and MBS, verifying the effectiveness and practicality of the proposed detection method.

In summary, the proposed detection method can effectively detect and extract the frequency of SRN under an ultra-low SNR threshold, and the detection effect is excellent. This will help improve the monitoring, reconnaissance, early warning, and protection capabilities in the marine field.

Appendix A: The general flow chart of the article



Acknowledgements

This work was supported by the Natural Science Foundation of Shaanxi Province (Grant No. 2026JC-YBMS-0747) and the National Natural Science Foundation of China (Grant No. 51709228).

References

[1] Yang H, Li J M, Li G H and Wang C 2025 *Eng. Appl. Artif. Intel.* **159** 111702
[2] Li G H, Wu M, Yang H 2025 *Appl. Acoust.* **239** 110809
[3] Lavezzo L, Gargano A, Scilingo E P and Nardelli M 2024 *Bioengineering-Basel* **11** 520
[4] Fu J B and Mu P H 2024 *J. Opt.* **26** 65704
[5] Li S Y, Tam L M, Wu S P, Tsai W L, Hu C W, Cheng L Y, Xu Y X and Cheng S C 2023 *Sensors* **23** 3801
[6] Chen Z G, Li Y A and Chen X 2015 *Acta Phys. Sin.* **64** 200502 (in Chinese)
[7] Zhang H W, Qin Z, Zhang Y C, Chen D J, Gen J and Qin H 2022 *EURASIP J. Wirel. Commun. Netw.* **2022** 41
[8] Hou J, Yan X P, Li P and Hao H X 2018 *Chin. Phys. B* **27** 30702
[9] Li G H, Zhang M Y and Yang H 2026 *Chaos Soliton Fract.* **207** 117915
[10] Wang K, Yan X P, Yang Q, Hao X H and Wang J T 2020 *J. Phys. Soc. Jpn.* **89** 14003
[11] Li G H, Xie R T and Yang H 2024 *Nonlinear Dyn.* **112** 2091
[12] Li G H, Zhao K X and Yang H 2025 *Chaos Soliton Fract.* **195** 116280
[13] Yang H, Liu Y X and Li G H 2025 *Eur. Phys. J. Plus* **140** 637
[14] Shen Y P, Li Y A, Li W J, Gao H L and Wu C L 2024 *Eur. Phys. J. Plus* **139** 325
[15] Shen Y P, Li Y A, Li W J, Gao H L and Wu C L 2024 *Digit. Signal Process.* **151** 104571
[16] Liu J M, Lin Z J and Wang W B 2019 *Eur. Phys. J. Plus* **134** 201
[17] Yan S H, Sun X, Wang Q Y, Ren Y, Shi W L and Wang E T 2021 *Phys. Scr.* **96** 125216
[18] Ding P F, Zhang J, Zhu J G, Geng P H and Hu W W 2025 *Phys. Scr.* **100** 075231
[19] Ding P F, Wang Z X, Li K and Yang L 2025 *Analog Integr. Circ. Signal Process.* **123** 15
[20] Ding P F, Geng P H, Hu W W, Zhang J and Zhu J G 2025 *Phys. Scr.* **100** 065207
[21] Ding P F, Hu W W, Geng P H, Zhang J and Zhu J G 2025 *J. Supercomput.* **81** 1201
[22] Tang Z Q, He S B, Wang H H, Sun K H, Yao Z and Wu X M 2024 *Chin. Phys. B* **33** 030503
[23] Rahman M U, Karaca Y, Agarwal R P and David S A 2024 *Appl. Math. Sci. Eng.* **32** 2300330
[24] Diabi L, Ouannas A, Hioual A, Momani S and Abbes A 2024 *Chin. Phys. B* **33** 100201

[25] Nabil H and Tayeb H 2024 *Chin. Phys. B* **33** 120503
[26] Wang J L, Wang Y L and Li X Y 2024 *J. Low Freq. Noise Vib. Act. Control* **43** 609
[27] Xu C J, Liao M X, Li P L, Yao L Y, Qin Q W and Shang Y L 2021 *Fract. Fract.* **5** 257
[28] Mao H C, Feng Y L, Wang X Q and Yao Z H 2024 *J. Nonlinear Math. Phys.* **31** 33
[29] Li G H, Xie R T and Yang H 2024 *Nonlinear Dyn.* **112** 17709
[30] Li G H, Xie R T and Yang H 2024 *Chaos Soliton Fract.* **186** 115255
[31] Wang J, Yu W X, Wang J N, Zhao Y M, Zhang J and Jiang D 2019 *Int. J. Circ. Theor. Appl.* **47** 702
[32] Ding P F, Li K and Wang Z X 2024 *Phys. Scr.* **99** 45221
[33] Li H, Li J, Fei H Z, Hong G Y, Dong J L and Yu A B 2024 *Mech. Syst. Signal Process.* **218** 111555
[34] He Y Z, Fu Y X and Qiao Z J 2021 *Chaos Soliton Fract.* **142** 110536
[35] Luo W M and Zhang Y R 2018 *Electron. Lett.* **54** 280
[36] Diethelm K, Ford N J and Freed A D 2002 *Nonlinear Dyn.* **29** 3
[37] Yang H, Liu Y X and Li G H 2025 *Chaos Soliton Fract.* **200** 117036
[38] Li G H, Xie Y C and Yang H 2026 *Measurement* **281** 121944
[39] Li G H, Du Y Q and Yang H 2026 *Def. Technol.*